OPEN

Facile Synthesis of Porous Polymer Using Biomass Polyphenol Source for Highly Efficient Separation of Cs$^+$ from Aqueous Solution

Shangqing Chen, Jiayin Hu✉, Yafei Guo & Tianlong Deng✉

In this work, a series of polyphenol porous polymers were derived from biomass polyphenols *via* a facile azo-coupling method. The structure and morphologies of the polymer were characterized by BET, TEM, SEM, XRD, TGA and FT-IR techniques. Batch experiments demonstrated their potentialities for adsorptive separation of Cs$^+$ from aqueous solution. Among them, porous polymers prepared with gallic acid as starting material (GAPP) could adsorb Cs$^+$ at wide pH value range effectively, and the optimal adsorption capacity was up to 163.6 mg/g, placing it at top material for Cs$^+$ adsorption. GAPP exhibited significantly high adsorption performance toward Cs$^+$ compared to Na$^+$ and K$^+$, making it possible in selective removal of Cs$^+$ from ground water in presence of co-existing competitive ions. Moreover, the Cs-laden GAPP could be facilely eluted and reused in consecutive adsorption-desorption processes. As a result, we hope this work could provide ideas about the potential utilization of biomass polyphenol in environmental remediation.

Growing concern about the remediation of radioactive waste generated from nuclear power plants and unforeseen accidents have been given worldwide for the sake of human health and environmental issues[1–4]. Among them, radio-isotope ^{137}Cs is considered as the most hazardous nuclide due to the serious gamma radiation, long half-life as well as high solubility being an alkaline element[5,6]. The generation of hazardous ^{137}Cs by nuclear waste and unforeseen nuclear plant accidents has seriously threatened the global environment and human health. In addition, long-term exposure to ^{137}Cs-containing wastewater would lead to horrible diseases such as cancer, leukemia and genetic disorder[7]. For example, the accidents occurred at Chernobyl in 1986 and Fukushima in 2011 severely impacted the local environments, and the surrounding areas are still classified as dangerous regions due to the leakage and serious emission of ^{137}Cs and other radio-isotopes[8,9]. Therefore, effective techniques for the decontamination of radioactive Cs$^+$ from wastewater are indispensable and highly desirable.

So far, considerable efforts have been made to explore available methodologies for hazardous Cs$^+$ removal from radioactive wastewater, such as liquid-liquid solvent extraction, chemical precipitation, electrochemical techniques and adsorption process[10–12]. Taking disposal cost and removal efficiency into consideration, adsorption is considered as one of the most effective and clean techniques, and has been widely used in Cs$^+$ removal. To date, Prussian blue (PB) analogues[12,13], titanate nanomaterials[14], metal oxides and sulfides[15], natural zeolites[16], ammonium molybdophosphate[17,18] and other adsorbents[19] were developed and used for the removal of Cs$^+$ from radioactive effluents. Unfortunately, they still suffered from several problems, such as considerable preparation cost, unsatisfactory adsorption performance and insufficient stability, thus majority of the adsorbents aforementioned were not environmental friendly, economically and industrially attractive. Therefore, the development of cost-effective, durable and effective Cs$^+$ adsorption materials are still particularly urgent.

More recently, it has been reported that resorcinol formaldehyde (RF) resin had a favorable affinity for Cs$^+$ due to the presence of phenolic hydroxyl groups[20], and Yang *et al*. demonstrated the phenolic hydroxyl exchange mechanism for Cs$^+$[21]. After that, easily available biomass materials with abundant polyphenolic groups have been used for Cs$^+$ adsorption. For example, Gurung and co-workers developed cross-linked persimmon tannin and tea leaves for Cs$^+$ removal, and it showed favorable selectivity and removal efficiency[22]. Pangeni *et al*. synthesized

Tianjin Key Laboratory of Brine Chemical Engineering and Resource Eco-utilization, College of Chemical Engineering and Materials Science, Tianjin University of Science and Technology, Tianjin, 300457, P.R. China. ✉e-mail: hujiayin@tust.edu.cn; tldeng@tust.edu.cn
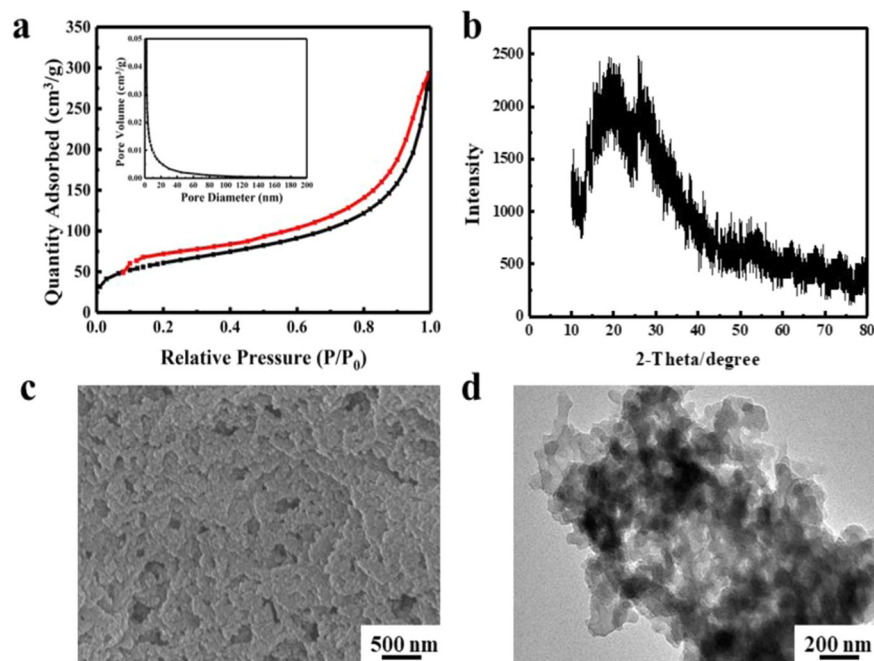
Figure 1. Characterization for the prepared GAPP: (**a**) N_2 adsorption-desorption isotherm, pore size distribution (inset); (**b**) XRD pattern; (**c**) SEM image; (**d**) TEM image.

a kind of cross-linked persimmon waste to uptake Cs^+ from wastewater and obtained an adsorption capacity of 71.8 mg/g[23]. Although the adsorbents prepared by cross-linking method showed good adsorption performance for Cs^+, however, the cross-linked persimmon tannin, tea leaves and persimmon waste adsorbents were difficult to recycle and reused, which were not economically attractive. Thus, further work are strongly desired to solve these problems.

Porous polymers (PPs) have been regarded as a kind of promising and unique materials, which have received considerable interests[24,25]. PPs can be designed to be with multiple functionalities by introducing various functional monomers, which endows them with novel properties and extensive applications in adsorption[26,27], separation[28,29], catalysis[30], hydrogen storage[31] and so on. To the best of our knowledge, there were negligible researches on the synthesis and application of PPs using biomass polyphenols sources on Cs^+ removal.

Herein, a series of polyphenol porous polymers were derived from biomass polyphenols sources *via* a facile azo-coupling method and provided a range of possibilities for Cs^+ separation from aqueous solution. Due to the porous structures functionalized by biomass polyphenols, the gallic acid-based porous polymer (GAPP) exhibited exceptionally adsorption performance for Cs^+ (163.6 mg/g). Moreover, this low-cost and environmentally friendly GAPP was robust in either acidic or basic solution (pH value range 2–12), and showed stable performance in consecutive adsorption-desorption experiments.

Results and Discussion
Characterization.   The N_2 adsorption-desorption isotherm (Fig. 1a) showed the porous structure of GAPP with a wide pore-size distribution (the inset in Fig. 1a, measured by Barret-Joyner-Halenda (BJH) method), and the specific surface area of 220 m^2/g and pore volume of 0.42 cm^3/g were calculated, respectively[32,33]. Due to the incomplete desorption in low pressure, there was a desorption hysteresis in N_2 isotherm. According to the isotherm classification system (IUPAC), the isotherm classification of GAPP was tend to Type II. Further SEM (Fig. 1c) and TEM (Fig. 1d) images also confirmed the porosity of GAPP, which was agreed with the results from N_2 adsorption. Additionally, XRD pattern (Fig. 1b) exhibited a broad peak, indicating the low crystallinity and amorphous structure of GAPP. FT-IR spectroscopy (Fig. 2a) showed that the IR frequencies appeared at 1608 and 3408 cm^{-1} indicated the presence of $-COO^-$ and $-O^-$ [34], and the bands at 1200 and 1400 cm^{-1} were attributed to the presence of the azo group, which proved the successful formation of the -N=N- band in the prepared GAPP[29,30]. The thermogravimetry analysis in Fig. 2b indicated the stable structure even in relatively high temperature (weight loss was less than 9.1% within 150 °C).

Adsorption performance.   A series of polyphenol porous polymers (PPs) were prepared using biomass polyphenols sources including phloroglucinol, tannic acid, arbutin and ellagic acid (Fig. 3) as starting materials, which were derived from biomass, such as persimmon, tea leaves, nut and so on. Their potentialities for Cs^+ adsorption were evaluated by batch experiments and the results are present in Fig. 4a. It was found that PPs obtained with different hydroxyl-containing starting materials were all efficient for Cs^+ adsorption. Especially, GAPP derived from gallic acid that had plentiful functional phenolic groups and weaker steric hindrance, showed
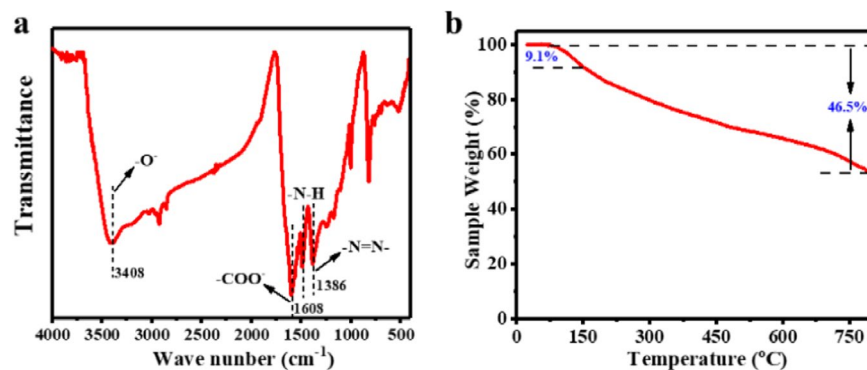
Figure 2. FT-IR spectrum (**a**) and thermogravimetric analysis (**b**) of GAPP.
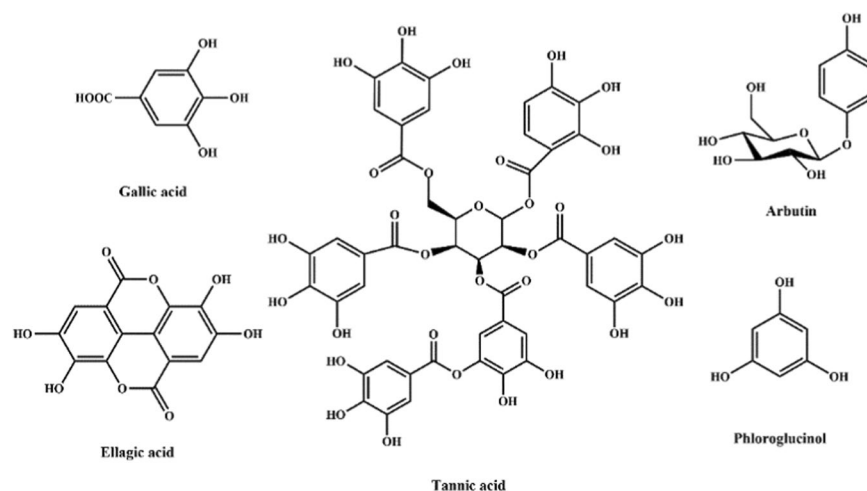
Figure 3. The structures of biomass polyphenols used in this work.

the best adsorption performance for Cs^+ than other PPs, indicating the great performance of gallic acid on Cs^+ adsorption. Therefore, GAPP was selected for further adsorption experiments hereafter.

Effect of pH value.   Firstly, the influence of pH value on the adsorption by GAPP was investigated, and the experiments were proposed with Cs^+ concentration of 100 mg/L and pH ranged from 2–12. As Fig. 4b showed, the GAPP was highly durable and could adsorb Cs^+ within pH ranging 2–12. Moreover, the q_e increased firstly when pH value increased from 2–6, and then decreased at pH value larger than 7.

The FT-IR data of GAPP before and after Cs^+ were compared in the Supporting Information (Fig. S1). It was found that the characteristic peak of -O- shifted to a slightly lower wavenumber after Cs^+ adsorption due to the coordination between -O- and the adsorbed Cs^+. This shifting was caused by the changes in force constants of the bonds as well as geometry of the O atoms after coordination[22,23]. Therefore, According to the experimental results and FT-IR spectra, the adsorption mechanism is proposed as Scheme 1.

When pH values were low, $-ONH_4$ group was likely to retain protons, thus resulting in insufficient adsorption sites and low adsorption capacity of GAPP for Cs^+. With the increase of pH values, $-ONH_4$ group was gradually transformed into $-O^-$. It could effectively interact with the polyphenolic groups of GAPP to form chelating cyclic metallacomplex, and the optimal adsorption capacity was achieved at pH 6.0. When pH values kept increasing, the adsorption capacity decreased because of much stronger ionic strength[35]. Moreover, there was electrostatic interaction between Cs^+ and $–O^-$ group. Therefore, the adsorption mechanism was considered to be coordination interaction and electrostatic interaction.

Effect of Cs^+ concentration and adsorption isotherms.   Adsorption isotherms are helpful to provide some information to describe the surface properties and the mechanism by which the interaction between the adsorbents and adsorbate[36]. Therefore, the adsorption capacities of GAPP were obtained by using different initial Cs^+ concentrations of solution (50~600 mg/L), and the equilibrium data were fitted using Langmuir and Freundlich isotherm models (further description see Supporting Information, S1.1)[36,37].

The experimental adsorption capacity of GAPP with different initial Cs^+ concentrations as well as the calculated curves are presented in Fig. 4c. It was found that the correlation coefficient of Langmuir isotherm model ($R^2 = 0.9899$) was bigger than that of Freundlich isotherm model ($R^2 = 0.9098$), meaning the adsorption mechanism was better described by the Langmuir isotherm model and the monolayer adsorption in the uniform surface
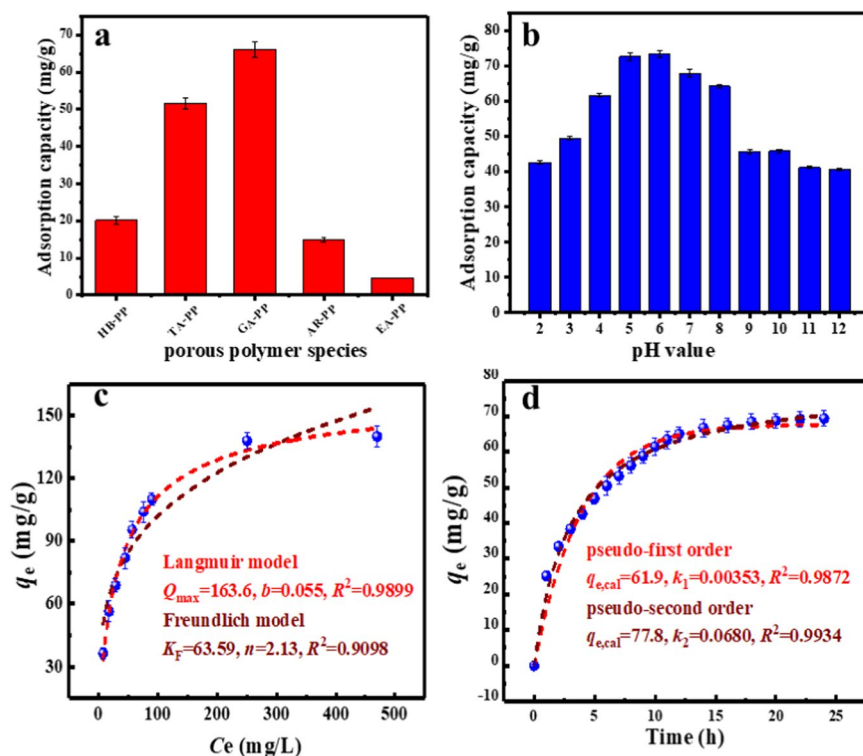
Figure 4. (**a**) Adsorption capacities of different PPs for Cs^+ ($C_0 = 100\,mg/L$, $m/V = 1\,g/L$, pH = 6.0, $t = 24\,h$, $T = 298.15\,K$); (**b**) Effect of pH value on Cs^+ adsorption by GAPP ($C_0 = 100\,mg/L$, $m/V = 1\,g/L$, $t = 24\,h$, $T = 298.15\,K$); (**c**) Effect of Cs^+ concentration and adsorption isotherm on adsorption ($C_0 = 0$–$500\,mg/L$, $m/V = 1\,g/L$, pH = 6.0, $t = 24\,h$, $T = 298.15\,K$); (**d**) Effect of contact time and adsorption kinetic on adsorption ($C_0 = 100\,mg/L$, $m/V = 1\,g/L$, pH = 6.0, $T = 298.15\,K$).
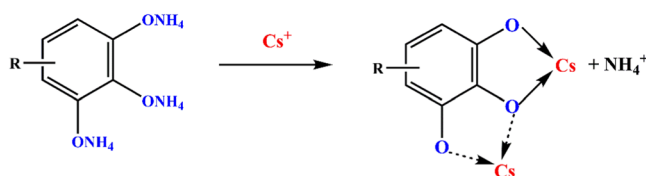
Scheme 1. The proposed adsorption mechanism of GAPP with Cs^+ (dotted arrow: electrostatic interaction; solid arrow: coordination interaction).

of GAPP. In addition, the value of n in Freundlich isotherm model was 2.13, which further suggested the favorable adsorption condition of Cs^+ on GAPP[34,38].

Effect of adsorption time and adsorption kinetics. The Cs^+ adsorption capacities *vs.* adsorption time were investigated with initial Cs^+ concentration of 100 mg/L, which are shown in Fig. 4d. The adsorption capacity increased rapidly because of the sufficient available binding sites of GAPP at the beginning, and then tended to be slower with the decreasing of the available GAPP binding sites and the Cs^+ concentration, and finally reached equilibrium within 24 h.

In this work, pseudo-first-order kinetic and pseudo-second-order kinetic model (S1.2) were used[39,40], and the experiment data and the fitting curves are shown in Fig. 4d. It was found that the adsorption process of Cs^+ on GAPP was better fitted by the pseudo-second-order model ($R^2 = 0.9882$) than pseudo-first-order model ($R^2 = 0.9672$), suggesting the major adsorption mechanism was chemisorption, and chemisorption was the rate-determining step, which was consistent with previous reports[22,23].

Effect of temperature and thermodynamics calculations. To figure out the effect of temperature on Cs^+ adsorption by GAPP, we carried out batch experiments under following conditions: initial Cs^+ concentration of 100 mg/L, pH value of 6.0 and temperature in the range of 298.15–328.15 K. In Fig. 5a, the q_e decreased slowly with the increasing of temperature, which suggested the exothermic nature of the adsorption process.

The correlation between $\ln K_d$ and $1/T$ would provide essential information about the calculation of ΔH^0 and ΔS^0 in the adsorption process[41]. According to Fig. 5b, the values of ΔH^0 and ΔS^0 were calculated to be $-17.08\,kJ\cdot mol^{-1}$ and $7.591\,J\cdot mol^{-1}\cdot K^{-1}$, respectively. Meanwhile, the values of ΔG^0 at different temperatures were
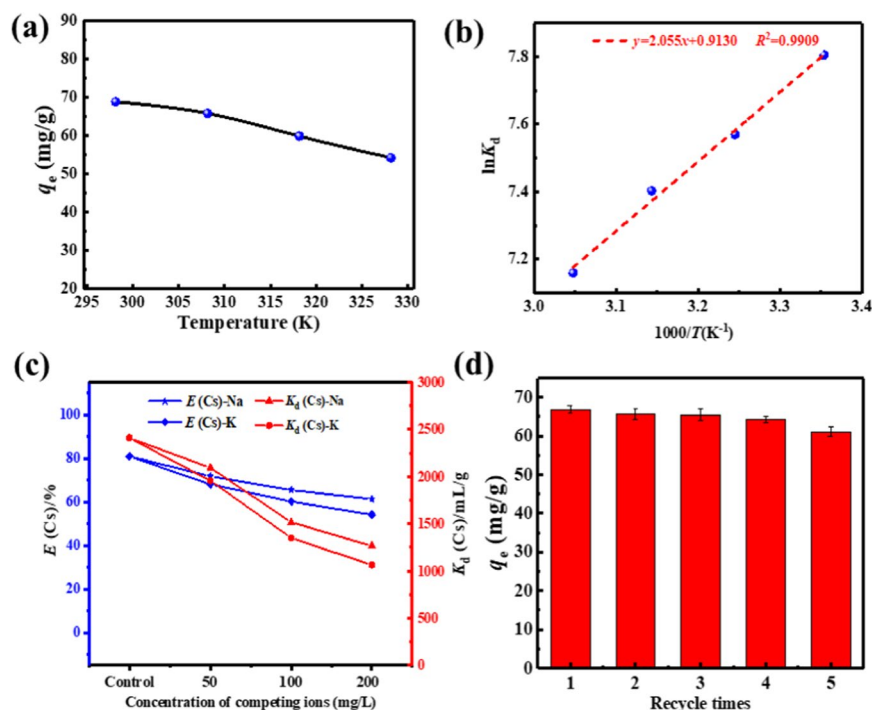
Figure 5. (**a**) Effect of temperature on Cs^+ adsorption ($C_0 = 100$ mg/L, $m/V = 1$ g/L, pH = 6.0, $t = 24$ h). (**b**) The Van't Hoff plot; (**c**) Effect of concentration of competing ions on Cs^+ adsorption ($C^{Cs}_0 = 100$ mg/L, $C^{Me}_0 = 0$–200 mg/L, $m/V = 1$ g/L, pH = 6.0, $t = 24$ h); (**d**) The recyclability of GAPP during consecutive adsorption-desorption process (adsorption: $C_0 = 100$ mg/L, $m/V = 1$ g/L, pH = 6.0, $T = 298.15$ K, $t = 24$ h; desorption: 1 mol/L NH_4Cl, $m/V = 1$ g/L, $T = 298.15$ K, 24 h).

	main metal cations				
	Cs^+	**Na^+**	**K^+**	**Ca^{2+}**	**Mg^{2+}**
Concentration (mg/L)	17.58	682.01	137.90	211.05	—
$E(\%)$	99.5	5.4	13.3	16.8	—
K_d (mL/g)	199000.2	57.1	153.4	201.9	—
S_F	1	3485.1	1297.3	985.6	—

Table 1. Concentrations of main metal cations in ground water and adsorption performance[a]. [a]GAPP dosage: 1 g/L, pH: 6.0, 298.15 K, 24 h.

obtained and given in Table S1. The negative value of ΔH^0 suggested the adsorption process belonged to exothermic process. In addition, the negative values of all the ΔG^0 at temperature ranging from 298.15–328.15 K indicated the cesium adsorption into GAPP was spontaneous and feasible, which further suggested the affinity of GAPP on cesium.

Effect of competitive cations on Cs^+ adsorption. The selectivity of GAPP is of significance in terms of the co-existing metal ions in wastewater, especially alkaline metal ions Na^+ and K^+, which are the most ubiquitous and similar elements with Cs^+. Therefore, the adsorption efficiency and distribution coefficient were determined in the presence of Na^+ and K^+ with different concentrations. The results are demonstrated in Fig. 5c, the adsorption efficiency and distribution coefficient gradually decreased with the increasing concentration Na^+ and K^+, and K^+ could retard the selective adsorption of Cs^+ on GAPP more seriously due to the closer similarity in hydration radius and chemical properties. However, the adsorption efficiency was about 20% less than that in pure Cs^+ solution, and the distribution coefficient was larger than 1000 mL/g at even high concentrations of competitive Na^+ or K^+ ions. Therefore, GAPP could be accepted as a selective adsorbent for Cs^+ adsorption.

Selective adsorption of Cs^+ from ground water. Considering that cesium generally enters water body from soil through different means, and to further evaluate the adsorption selectivity of GAPP over Cs^+, selective experiments were studied using ground water, whose compositions of main metal cations, adsorption efficiency and distribution coefficients are presented in Table 1. The Cs^+ adsorption efficiency could reach 99.5% and those for other metal cations were less than 16.8% after a simple absorption process. The distribution coefficient for Cs^+ was about 2×10^5 mL/g, which was much larger than some existing Cs^+ adsorbents. As a result, the separation factors S_F of Cs^+ over Na^+, K^+ and Ca^{2+} were 3485.1, 1297.3 and 985.6, respectively. The results above further

Materials	Adsorption capacity (mg/g)	Active pH range[a]	Selectivity	Reusability	Ref.
CPT gel	178.2	2.5–6.5	*vs.* Na$^+$,	Limited	[22]
CTL gel	162.3	3–6	*vs.* Na$^+$	Limited	[22]
CPW gel	71.8	2.5–7.5	—	Limited	[23]
SSM	52.4	2–12	*vs.* Na$^+$, K$^+$	Reusable	[42]
Bn-CTS	57.1	3–10	*vs.* Li$^+$, Na$^+$, K$^+$, Mg^{2+}	Reusable	[43]
MgP-MS	64.0	5–10	—	Reusable	[44]
Magnetic 4 A zeolite	106.6	—	—	—	[45]
Fe$_3$O$_4$-O-CMK-3	205	3–11	*vs.* Li$^+$, Na$^+$, K$^+$, Ca^{2+}, Sr^{2+}	Reusable	[46]
mag-AMP	83.33	2–12	—	Reusable	[41]
MMT-PB	57.47	—	*vs.* Na$^+$, K$^+$, Mg^{2+}, Ca^{2+}	—	[47]
GAPP	**163.6**	**2–12**	***vs.* Na$^+$, K$^+$**	**Reusable**	**this work**

Table 2. Comparison of various Cs$^+$ adsorbents in the literature and GAPP. ^{a}pH range in which the adsorbents could maintain more than 50% of the maximum adsorption capacity[48,49].

suggested that GAPP showed an efficient adsorption performance and selectivity for Cs$^+$ over Na$^+$, K$^+$ from ground water with complex competitive cations. Therefore, this GAPP could be accepted as a selective material with potential use on Cs$^+$ removal from radioactive wastewater in presence of competitive cations.

Desorption and reusability. To investigate the recycle performance of GAPP, the consecutive adsorption-desorption processes were carried out using NH$_4$Cl solution as the eluent. As Fig. 5d shows, the adsorption capacity decreased slightly from 66.9 mg/g to 61.1 mg/g (decreased for about 8.6%) after being reused five times, indicating that the stable performance of GAPP in consecutive adsorption-desorption experiments. Furthermore, FT-IR and EDX analysis of GAPP after five-time recycle were carried out to demonstrate its stability during adsorption and desorption processes. To our delight, it was found that the FT-IR spectrum after adsorption (as Fig. S1b) was similar with that of original adsorbent (Fig. S1a) and further EDX analysis in Table S2 also indicated the favorable stability of GAPP during adsorption and desorption processes.

Comparison of GAPP with other adsorbents. A comparison of GAPP and other materials was conducted to assess the potential application of GAPP From Table 2, we could find that the obtained adsorption capacity of GAPP (163.6 mg/g) on Cs$^+$ was much larger than some biomass-based adsorbents, such as CPW gel (71.8 mg/g), SSM (52.4 mg/g), Bn-CTS (57.1 mg/g), MgP-MS (64.0 mg/g), and comparable with CPT gel (178.2 mg/g) and CPW gel (162.3 mg/g). However, CPT gel and CPW gel could only be effective at a narrow pH rang (3–6), and they could not be recycled and reused. Compared with other inorganic adsorbents, the selectivity and adsorption capacity of GAPP was also outstanding at a broad pH range (2–12). Furthermore, it was selective over alkaline metals Na$^+$ and K$^+$ in ground water and shows stable performance during consecutive adsorption-desorption experiments. Therefore, we believe this cost-effective, robust and efficient adsorbent can be accepted as an effective material with potential application in Cs$^+$ removal from radioactive wastewater.

Conclusions

In this work, cost-effective and robust porous polymers were fabricated using biomass polyphenol sources *via* a facile azo-coupling method and applied for Cs$^+$ separation from aqueous solutions. Due to the porous structures functionalized by biomass polyphenols, the gallic acid-based porous polymer (GAPP) exhibited stable performance at wide pH value range with a maximum adsorption capacity of 163.6 mg/g, placing it at top material for Cs$^+$ adsorption. More importantly, GAPP showed significantly high adsorption performance toward Cs$^+$ compared to Na$^+$ and K$^+$, making it possible in selective removal of Cs$^+$ from ground water in presence of co-existing competitive ions. In addition, the Cs-laden GAPP could be facilely eluted and reused in consecutive adsorption-desorption process. Therefore, we believe that this low-cost, robust and selective GAPP is a promising material with potential application on ^{137}Cs removal from radioactive wastewater, and we hope this work could provide more ideas about the potential utilization of biomass polyphenols in representative fields.

Materials and Methods

Chemicals and materials. Gallic acid (GA, 98%), tannic acid (TA, 95%), 1,3,5-trihydroxybenzene (phloroglucinol, HB, 99%) were supplied by J & K Scientific Ltd. Ellagic acid (EA, 98%) and arbutin (AR, 98%) were obtained from Macklin Biochemical Co., Ltd. Benzidine (BE, 98%) was obtained from Aladdin. Cesium chloride, sodium nitrite, sodium carbonate and other regents were provided by Tianjin Guangfu Reagent. Ground water sampled from Tibet, China was used for adsorption performance evaluation of the adsorbents.

Preparation of porous polymers. The GAPP was prepared using gallic acid as starting material, and the synthesis procedure was shown as Scheme 2 for example, and those for other PPs were similar. BE (5 mmol) was firstly dissolved in 5% HCl solution, and NaNO$_2$ solution (10 mmol) was then added and stirred for 30 min. After that, the solution was contacted with a mixture of GA (3 mmol) and Na$_2$CO$_3$ (12 mmol) at ice-water mixture.
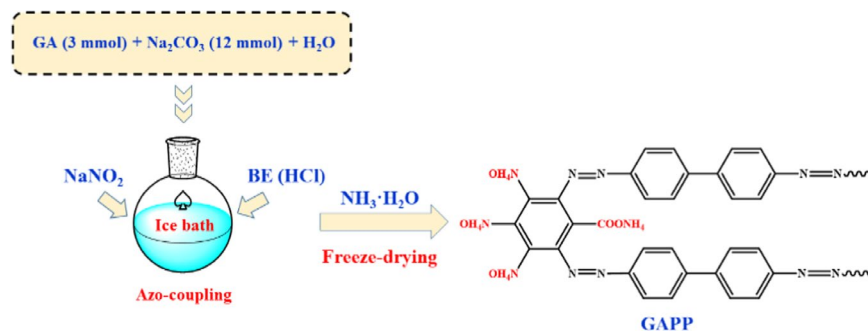
Scheme 2. Preparation roadmap of GA.

After reaction for 12 h, the mixtures were separated by simple centrifugation for 30 min (Z326, Germany) and washed by H_2O and ethanol. Subsequently, it was subjected to $NH_3 \cdot H_2O$ solution for about 12 h. Finally, it was washed by water for three times and freeze-drying for further use.

Instrumentation. FT-IR spectroscopy (Tensor 27, Germany) was used to identify the groups in the materials. Powder X-ray diffraction (XRD) were collected on X-ray diffractometer with Cu Kα radiation (MSAL XD-3, China). The thermal property of GAPP was evaluated using a thermogravimetric analysis (TGA) instrument (Seteram Labsys, France) over the temperature range of 30–800 °C under Ar atmosphere at 10 °C/min heating rate. The surface properties of GAPP was characterized by SEM (JSM-IT300LV, Japan). The transmission electron microscopy (TEM) image was determined by a TEM JEM-1011. The elemental compositions were determined by EDX (X-Max 20, Oxford Instruments). The N_2 adsorption-desorption isotherms were obtained using a physical adsorption analyzer (ASAP 2020, Micromeritics) and the surface area was obtained by the BET method.

Batch experiments. In each experiment, the desired amounts of adsorbents and Cs^+ solution with given initial concentrations were loaded in a polytetrafluoroethylene bottle, and then it was shaken in a thermostat with certain temperature. After that, it was stopped and centrifuged to take the clarified supernatant for chemical analysis. The concentrations of metallic ions were determined by ICP-OES. Moreover, the detailed experimental conditions were described in the figures and tables captions. The key parameters during the adsorption, such as adsorption efficiency (E, %), adsorption capacity (q_t, mg/g), distribution coefficient (K_d, mL/g) and separation factor (S_F) were calculated by Eqs. 1–4.

$$E(\%) = \frac{C_0 - C_t}{C_0} \times 100 \tag{1}$$

$$q_t(\text{mg/g}) = \frac{(C_0 - C_t)V}{m} \tag{2}$$

$$Kd\ (\text{mL/g}) = \frac{(C0 - Ce)}{Ce} \times \frac{1000V}{m} \tag{3}$$

$$S_F = \frac{Kd^{Cs}}{Kd^{Me}} \tag{4}$$

where C_0, C_t and C_e (mg/L) represent the original, final and the equilibrium concentrations of Cs^+; V (L) refers to the aqueous solution volume; m (g) represents the mass of the adsorbent; Me are different competitive cations.

References

1. Yang, D. J. *et al*. Capture of radioactive cesium and iodide ions from water by using titanate nanofibers and nanotubes. *Angew. Chem. Int. Ed.* **50**, 10594–10598 (2011).
2. Sarina, S. *et al*. Separate or simultaneous removal of radioactive cations and anions from water by layered sodium vanadate-based sorbents. *Chem. Mater.* **26**, 4788–4795 (2014).
3. Wen, T. *et al*. Multifunctional flexible free-standing titanate nanobelt membranes as efficient sorbents for the removal of radioactive $^{90}Sr^{2+}$ and $^{137}Cs^+$ ions and oils. *Sci. Rep* **6**, 20920 (2016).
4. Zou, Y. *et al*. Environmental remediation and application of nanoscale zero-valent iron and its composites for the removal of heavy metal ions: A review. *Environ. Sci. Technol.* **50**, 7290–7304 (2016).
5. Torad, N. L., Hu, M., Imura, M., Naito, M. & Yamauchi, Y. Large Cs adsorption capability of nanostructured prussian blue particles with high accessible surface areas. *J. Mater. Chem.* **22**, 18261–18267 (2012).
6. Kim, H., Kim, M., Lee, W. & Kim, S. Rapid removal of radioactive cesium by polyacrylonitrile nanofibers containing prussian blue. *J. Hazard. Mater.* **347**, 106–113 (2018).

7. Zhang, A., Dai, Y., Xu, L. & Chai, Z. Solvent extraction of cesium with a new compound calix[4] arene-bis[(4-methyl-1,2-phenylene)-crown-6]. *J. Chem. Eng. Data* **58**, 3275–3281 (2013).
8. Castrillejo, M. *et al.* Reassessment of ^{90}Sr, ^{137}Cs, and ^{134}Cs in the coast off Japan derived from the Fukushima Dai-ichi nuclear accident. *Environ. Sci. Technol.* **50**, 173–180 (2016).
9. Schmid, S. Midnight in Chernobyl: The untold story of the World's greatest nuclear disaster. *Nature* **566**, 450–451 (2019).
10. Banerjee, D., Rao, M. A. & Wattal, P. K. Separation and recovery of Cs from high active waste simulant using resorcinol formaldehyde polycondensate resin: batch and column studies. *Sep. Sci. Technol* **48**, 133–139 (2013).
11. Alby, D., Charnay, C., Heran, M., Prelot, B. & Zajac, J. Recent developments in nanostructured inorganic materials for sorption of cesium and strontium: synthesis and shaping, sorption capacity, mechanisms, and selectivity-a review. *J. Hazard. Mater.* **344**, 511–53 (2018).
12. Wang, J. L., Zhuang, S. T. & Liu, Y. Metal hexacyanoferrates-based adsorbents for cesium removal. *Coordination Chem. Rev.* **374**, 430–438 (2018).
13. Cho, E., Kim, J., Park, C. W., Lee, K. W. & Lee, T. S. Chemically bound prussian blue in sodium alginate hydrogel for enhanced removal of Cs ions. *J. Hazard. Mater.* **360**, 243–249 (2018).
14. Feng, M. L. *et al.* Efficient removal of [UO2]$^{2+}$, Cs$^+$, and Sr^{2+} ions by radiationresistant gallium thioantimonates. *J. Am. Chem. Soc.* **140**, 11133–11140 (2018).
15. Manos, M. J. & Kanatzidis, M. G. Highly efficient and rapid Cs$^+$ uptake by the layered metal sulfide K$_{2x}$Mn$_x$Sn$_{3-x}$S$_6$ (KMS-1). *J. Am. Chem. Soc.* **6**, 6599–6607 (2009).
16. Baek, W., Ha, S., Hong, S., Kim, S. & Kim, Y. Cation exchange of cesium and cation selectivity of natural zeolites: chabazite, stilbite, and heulandite. *Micropor. Mesopor. Mater* **264**, 159–166 (2018).
17. Deng, H., Li, Y. X., Wu, L. & Ma, X. The novel composite mechanism of ammonium molybdophosphate loaded on silica matrix and its ion exchange breakthrough curves for cesium. *J. Hazard. Mater.* **324**, 348–356 (2017).
18. Han, E., Kim, Y. G., Yang, H. M., Yoon, I. H. & Choi, M. Synergy between zeolite framework and encapsulated sulfur for enhanced ion-exchange selectivity to radioactive cesium. *Chem. Mater.* **30**, 5777–5785 (2018).
19. Ding, N. & Kanatzidis, M. G. Selective incarceration of caesium ions by Venus flytrap action of a flexible framework sulfide. *Nat. Chem* **2**, 187–191 (2010).
20. Dwivedi, C. *et al.* Resorcinol-formaldehyde coated XAD resin beads for removal of cesium ions from radioactive waste: synthesis, sorption and kinetic studies. *RSC Adv* **2**, 5557–5564 (2012).
21. Yang, S. B., Han, C., Wang, X. K. & Nagatsu, M. Characteristics of cesium ion sorption from aqueous solution on bentonite- and carbon nanotube-based composites. *J. Hazard. Mater.* **274**, 46–52 (2014).
22. Gurung, M. *et al.* Adsorptive removal of Cs(I) from aqueous solution using polyphenols enriched biomass-based adsorbents. *Chem. Eng. J* **231**, 113–120 (2013).
23. Pangeni, B. *et al.* Preparation of natural cation exchanger from persimmon waste and its application for the removal of cesium from water. *Chem. Eng. J* **242**, 109–116 (2014).
24. Slater, A.G., Cooper, A.I. Function-led design of new porous materials, *Science* **348** (2015).
25. Xu, Y. H., Jin, S. B., Xu, H., Nagai, A. & Jiang, D. L. Conjugated microporous polymers: design, synthesis and application. *Chem. Soc. Rev.* **42**, 8012–8031 (2013).
26. Li, A. *et al.* Lithium-doped conjugated microporous polymers for reversible hydrogen storage. *Angew. Chem. Int. Ed* **49**, 3330–3333 (2010).
27. Neti, V. S. P. K., Wang, J., Deng, S. G. & Echegoyen, L. High and selective CO$_2$ adsorption by a phthalocyanine nanoporous polymer. *J. Mater. Chem. A* **3**, 10284–10288 (2015).
28. Zhang, Y. G. & Riduan, S. N. Functional porous organic polymers for heterogeneous catalysis. *Chem. Soc. Rev.* **41**, 2083–2094 (2012).
29. Ji, G. P. *et al.* Hierarchically mesoporous o-hydroxyazobenzene polymers: synthesis and their applications in CO$_2$ capture and conversion. *Angew. Chem. Int. Ed* **55**, 9685–9689 (2016).
30. Xie, C. *et al.* Naturally occurring gallic acid derived multifunctional porous polymers for highly efficient CO$_2$ conversion and I$_2$ capture. *Green Chem.* **20**, 4655–4661 (2018).
31. Dang, Q. Q., Wang, X. M., Zhang, Y. F. & Zhang, X. M. An azo-linked porous triptycene network as an absorbent for CO$_2$ and iodine uptake. *Polymer Chem* **7**, 643–647 (2016).
32. Patra, A. K., Das, S. K. & Bhaumik, A. Self-assembled mesoporous TiO$_2$ spherical nanoparticles by a new templating pathway and its enhanced photoconductivity in the presence of an organic dye. *J. Mater. Chem.* **21**, 3925–3930 (2011).
33. Dutta, A., Patra, A. K., De, S., Bhaumik, A. & Saha, B. Self-assembled TiO$_2$ nanospheres by using a biopolymer as a template and its optoelectronic application. *ACS Appl. Inter. Mater* **4**, 1560–1564 (2012).
34. Chen, S. Q. *et al.* Composite hydrogel particles encapsulated ammonium molybdophosphate for efficiently cesium selective removal and enrichment from wastewater. *J. Hazard. Mater.* **371**, 694–704 (2019).
35. Zhu, Y. F. *et al.* Fabrication of a magnetic porous hydrogel sphere for efficient enrichment of Rb$^+$ and Cs$^+$ from aqueous solution. *Chem. Eng. Res. Des.* **125**, 214–225 (2017).
36. Olatunji, M. A., Khandaker, M. U., Mahmud, H. E. & Amin, Y. M. Influence of adsorption parameters on cesium uptake from aqueous solutions-a brief review. *RSC Adv* **5**, 71658–71683 (2015).
37. Freundlich, H. M. F. Über die adsorption in Lösungen. *Z. Phys. Chem.* **57A**, 385–470 (1906).
38. Lu, T. T., Zhu, Y. F., Wang, W. B., Qi, Y. X. & Wang, A. Q. Interconnected superporous adsorbent prepared via yeast-based Pickering HIPEs for high-efficiency adsorption of Rb$^+$, Cs$^+$ and Sr^{2+}. *Chem. Eng. J.* **361**, 1411–1422 (2019).
39. Kumar, P. A., Ray, M. & Chakraborty, S. Adsorption behaviour of trivalent chromium on amine-based polymer aniline formaldehyde condensate. *Chem. Eng. J* **149**, 340–347 (2009).
40. Nur, T., Loganathan, P., Kandasamy, J. & Vigneswaran, S. Removal of strontium from aqueous solutions and synthetic seawater using resorcinol formaldehyde polycondensate resin. *Desalination* **420**, 283–291 (2017).
41. Yang, H. J. *et al.* Facile synthesis of mesoporous magnetic AMP polyhedric composites for rapid and highly efficient separation of Cs$^+$ from water. *Chem. Eng. J* **317**, 533–543 (2017).
42. Khandaker, S., Toyohara, Y., Kamida, S. & Kuba, T. Effective removal of cesium from wastewater solutions using an innovative low-cost adsorbent developed from sewage sludge molten slag. *J. Environ. Manage.* **222**, 304–315 (2018).
43. Wang, K. X. *et al.* Hybrid porous magnetic bentonite-chitosan beads for selective removal of radioactive cesium in water. *J. Hazard. Mater.* **362**, 160–169 (2018).
44. El-Din, A. F. T., El-Khouly, M. E., Elshehy, E. A., Atia, A. A. & El-Said, W. A. Cellulose acetate assisted synthesis of worm-shaped mesopores of MgP ion-exchanger for cesium ions removal from seawater. *Micropor. Mesopor. Mater* **265**, 211–218 (2018).
45. Wang, W. Q. *et al.* A novel magnetic 4A zeolite adsorbent synthesized from kaolinite type pyrite cinder (KTPC). *Solid State Sci* **39**, 52–58 (2014).
46. Husnain, S. M., Um, W., Chang, Y. Y. & Chang, Y. S. Recyclable superparamagnetic adsorbent based on mesoporous carbon for sequestration of radioactive cesium. *Chem. Eng. J* **308**, 798–808 (2016).
47. Alamudy, H. A. & Cho, K. Selective adsorption of cesium from an aqueous solution by a montmorillonite-prussian blue hybrid. *Chem. Eng. J* **349**, 596–602 (2018).
48. Park, Y., Lee, Y. C., Shin, W. S. & Choi, S. J. Removal of cobalt, strontium and cesium from radioactive laundry wastewater by ammonium molybdophosphate-polyacrylonitrile (AMP-PAN). *Chem. Eng. J* **162**, 685–695 (2010).
49. Langmuir, I. The adsorption of gases on plane surface of glass, mica and platinum. *J. Am. Chem. Soc.* **40**, 1361–1403 (1918).

Author contributions

S.Q. Chen and J.Y. Hu conceived the study design and conducted the experiment, Y.F. Guo and T.L. Deng analyzed the results, S.Q. Chen and T.L. Deng wrote the final manuscript. All authors reviewed the manuscript.

Competing interests

The authors declare no competing interests.

Additional information

Supplementary information is available for this paper at https://doi.org/10.1038/s41598-020-65099-6.

Correspondence and requests for materials should be addressed to J.H. or T.D.

Reprints and permissions information is available at www.nature.com/reprints.

Publisher's note Springer Nature remains neutral with regard to jurisdictional claims in published maps and institutional affiliations.